

High Spatial Resolution Spectroscopy of G292.0+1.8 with *Chandra* *

Xue-Juan Yang¹, Xiaoqin Liu¹, Shun-yu Li¹ and Fang-Jun Lu²

¹ Faculty of Materials, Optoelectronics and Physics, Xiangtan University, Xiangtan 411105, China;
xjyang@xtu.edu.cn

² Particle Astrophysics Center, Institute of High Energy Physics, Chinese Academy of Sciences,
 Beijing 100049, China

Received [year] [month] [day]; accepted [year] [month] [day]

Abstract We present high spatial resolution X-ray spectroscopy of supernova remnant G292.0+1.8 with the *Chandra* observations. The X-ray emitting region of this remnant was divided into 25×25 pixels with a scale of $20'' \times 20''$ each. Spectra of 324 pixels were created and fitted with an absorbed one component non-equilibrium ionization model. With the spectral analysis results we obtained maps of absorbing column density, temperature, ionization age, and the abundances for O, Ne, Mg, Si, S, and Fe. The abundances of O, Ne and Mg show tight correlations between each other in the range of about two orders of magnitude, suggesting them all from explosive C/Ne burning. Meanwhile, the abundances of Si and S are also well correlated, indicating them to be the ashes of explosive O-burning or incomplete Si-burning. The Fe emission lines are not prominent among the whole remnant, and its abundance are significantly deduced, indicating that the reverse shock may have not propagated to the Fe-rich ejecta. Based on relative abundances of O, Ne, Mg, Si and Fe to Si, we suggest a progenitor mass of $25 - 30 M_{\odot}$ for this remnant.

Key words: ISM: supernova remnants – ISM: individual: G292.0+1.8

1 INTRODUCTION

G292.0+1.8, also known as MSH 11-54, is a bright Galactic supernova remnant (SNR). It is relatively young with the age of $\leq 1600 \text{ yr}$ (Murdin & Clark 1979). The detection of strong O and Ne lines in the optical spectrum (Goss et al. 1979; Murdin & Clark 1979) classified G292.0+1.8 as one of the only three known O-rich SNRs in the Galaxy, the others being Cassiopeia A and Puppis A.

G292.0+1.8 was first detected in X-ray with *HEAO 1* (Share et al. 1978). With the increasing sensitivity and resolution of the following X-ray satellites, finer structures are revealed, such as the central bar-like features (Tuohy, Clark, & Burton 1982), metal rich ejecta around the periphery, thin filaments with normal composition centered on and extending nearly continuously around the outer boundary (Park et al. 2002). The equivalent width map of O, Ne, Mg, Si clearly show regions with enhanced metallicity of these elements (Park et al. 2002). G292.0+1.8 is bright in O, Ne, Mg and Si and weaker in S and Ar with little Fe, suggesting that the ejecta are strongly stratified by composition and that the reverse shock has not propagated to the Si/S- or Fe-rich zones (Park et al. 2004; Ghavamian et al.

* Supported by the National Natural Science Foundation of China.

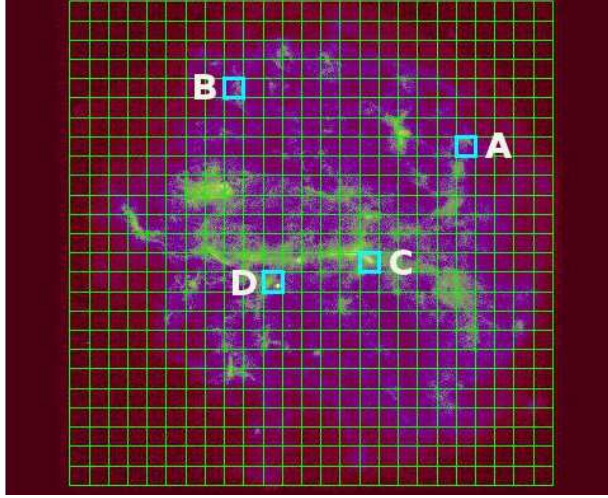


Fig. 1 The pixel grid used in our analyses superimposed on the *Chandra* image of G292.0+1.8.

2012). Meanwhile, the central barlike belt has normal chemical composition, suggesting shocked dense circumstellar material for its origin (Park et al. 2004; Ghavamian, Hughes & Williams 2005).

The detection of the central pulsar (PSR J1124–5916) and its wind nebula (Hughes et al. 2001, 2003; Camilo et al. 2002; Gaensler & Wallace 2003; Park et al. 2007) attribute G292.0+1.8 to be a core-collapse SNR. The progenitor mass has been proposed. Hughes & Singh (1994) suggested a progenitor mass of $\sim 25 M_{\odot}$ by comparing the derived element abundances of O, Ne, Mg, Si, S and Ar with those predicted by the numerical nucleosynthesis calculation based on the *EXOSAT* data. Gonzalez & Safi-Harb (2003) estimated it to be $\sim 30 - 40 M_{\odot}$ with the same method from *Chandra* observation.

In this paper, we present a spatially resolved spectroscopy of G292.0+1.8, using *Chandra* ACIS observations. In previous work, several typical regions have been picked out and their spectra were analyzed (e.g. Gonzalez & Safi-Harb 2003, hereafter GS03; Vink et al. 2004; Lee et al. 2010) or the equivalent width maps are given (Park et al. 2002). We, for the first time, give a systematic spectroscopy of this SNR region by region. In Section 2 & 3, we present observational data and results. In Section 4, we discuss the nucleosynthesis and progenitor mass. A summary is given in Section 5.

2 OBSERVATION AND DATA REDUCTION

G292.0+1.8 was observed by ACIS-S3 chip on board *Chandra* on 2000-03-11 from 00:05:46 to 13:21:46 UTC with observation ID 126. After screening the data, the net exposure time is about 43 ks.

The X-ray data were analyzed using the software package CIAO (version 4.1). In this paper, we divided the X-ray emission region into 25×25 grids with “pixel” size of $20'' \times 20''$. We extracted events within energy range 0.5–10 keV and created spectra for 328 pixels. Figure 1 shows the image of this observation with the grid overlaid. The background spectrum was created from the off-source region.

The spectra were fitted within XSPEC software package (version 11.3, Arnaud 1996), using one non-equilibrium ionization component (VNEI, Borkowski et al. 2001). The free parameters are the temperature, emission measure, ionization age ($\tau = n_e t$) and abundances of O, Ne, Mg, Si, S, Fe (in units of solar abundances given by Anders & Grevesse (1989)). The reason these elements’ abundances being free is that they show prominent emission lines in the spectra (cf. Figure 3). We also introduced the WABS model (Morrison & MacCammon 1983) for the interstellar photoelectric absorption.

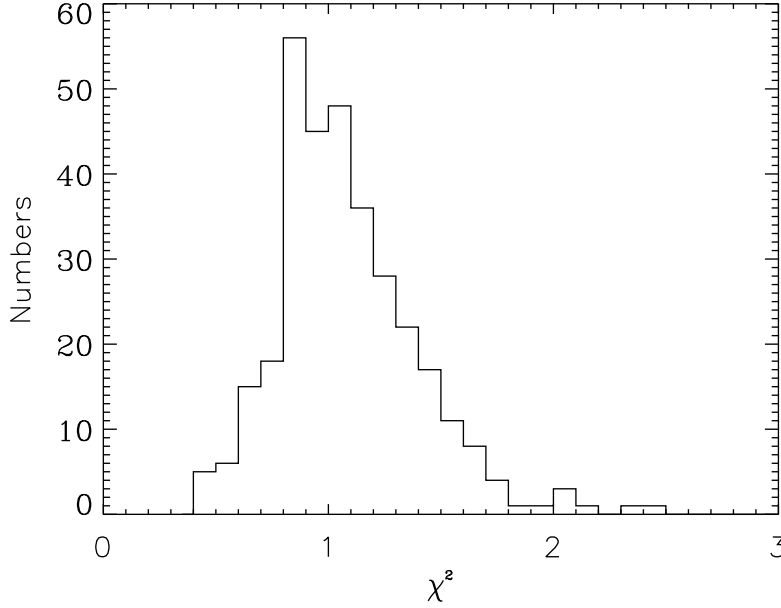


Fig. 2 Frequency distribution of the 328 pixel χ^2 values obtained in the spectra fitting.

3 RESULTS

Figure 2 shows the frequency distribution of the 328 reduced χ^2 values of the spectral fits, which peaks around 0.85, suggesting the fitting results to be acceptable statistically.

In Figure 3, we give the spectra along with the fitting residuals of several typical regions (marked in Figure 1). Region A is the O/Ne-rich region, with strong O and Ne lines and very weak Si, S lines. The abundance for O, Ne and Mg are above 4.0 while ≤ 0.3 for Si and S. As an O-rich SNR, such a region is very typical. Region B, on the other hand, shows strong Si and S lines, and relatively weak O and Ne lines. It has a much higher abundance for Si and S (~ 2.0), and much smaller abundance for O, Ne and Mg (~ 3.0) than region A. Region C is from the central bright belt area, which shows very strong continuum and medium-mass emission lines. The abundance for all the metal elements are significantly deduced (0.3 – 0.5). Region D covers the central pulsar. A very strong hard continuum tail is observed from the spectrum. O, Ne and Mg lines are clearly shown while no emission lines above 1.8 keV. Fe-K lines, however, are not detected in any of these regions.

The emission lines from O can be detected in O-rich (A), Si-rich region (B), and even pulsar-dominate region (D). However, the central bar-like feature (such as region C), although very bright it is, shows very weak O emission line. This supports that such a belt should originate from the shocked circumstellar medium, rather than metal-rich ejecta (Park et al. 2002). The hard tail in the spectrum of region D is due to the pulsar. The photon index is 1.87 ± 0.09 , which is consistent with the value given by GS03 (1.74 ± 0.10) and Hughes et al. (2003; 1.6) and the typical photon index of a pulsar (1.5–2.0, Becker 2009).

(I) The spatial distribution of the fitted parameters.

The spatial distribution of the absorbing column density, temperature and the ionization ages are shown in Figure 4. The column density to this SNR lies in the range $0.2 - 0.7 \times 10^{22} \text{ cm}^{-2}$, with the mean value $\sim 0.45 \times 10^{22} \text{ cm}^{-2}$. This is consistent with previous results (Park et al. 2004). The

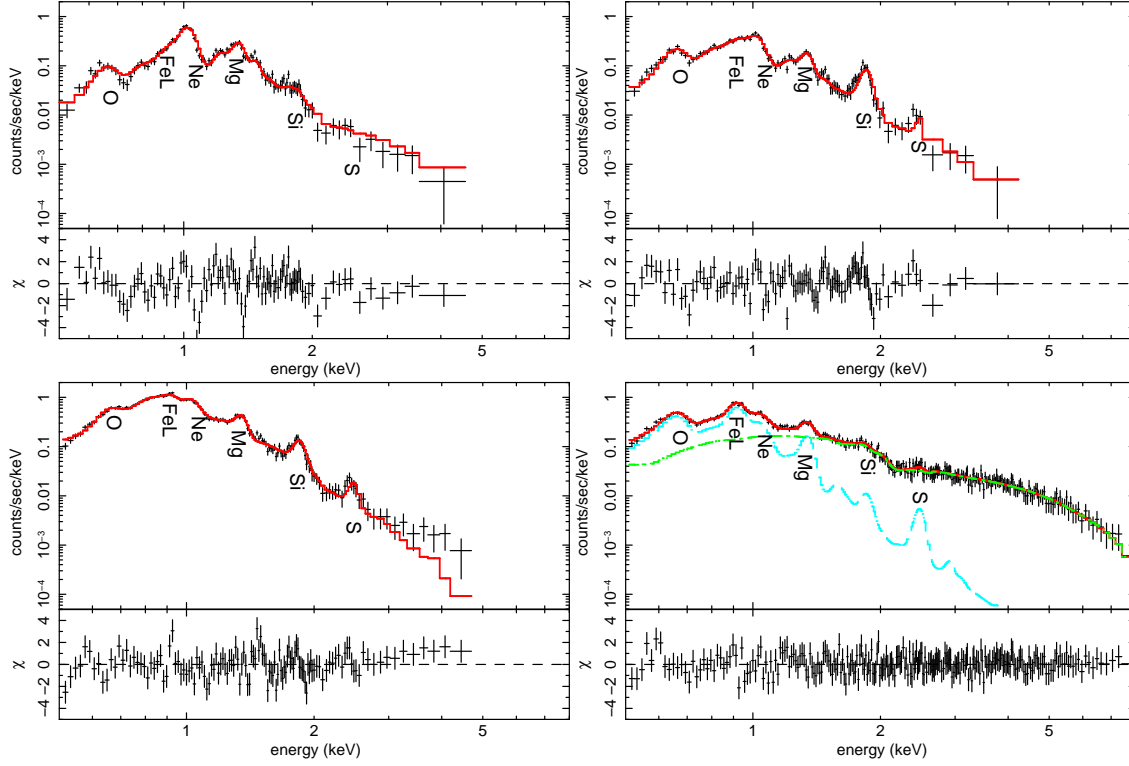


Fig. 3 Spectra along with the fitting results for typical regions as denoted in Figure 1. Region A: top left; Region B: top right; Region C: bottom left; Region D: bottom right.

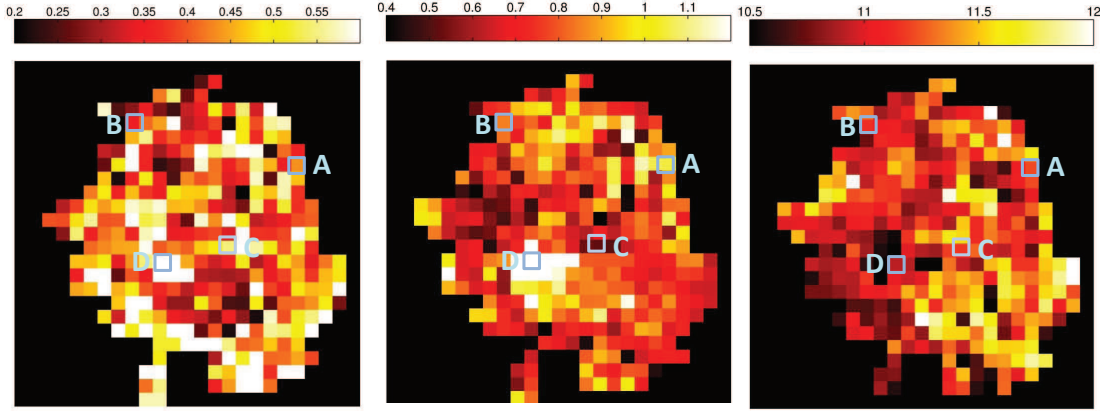


Fig. 4 The absorbing column density (N_H , 10^{22} cm^{-2} , left panel), temperature (kT , keV , middle panel) and ionization age ($\text{Log}_{10} n_e t \text{ cm}^{-3} \text{ s}$, right panel) maps of G292.0+1.8. The coding used is shown on the top of each panel. Regions A/B/C/D as shown in Figure 1 are marked here.

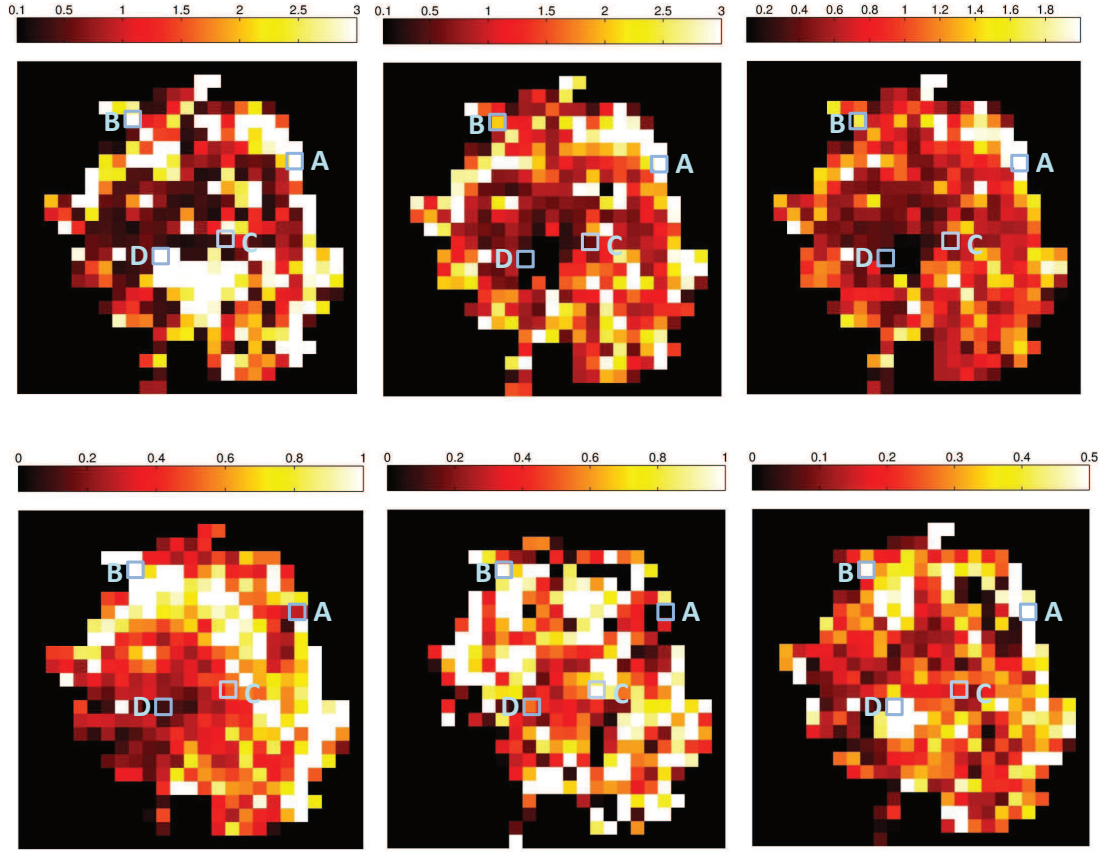


Fig. 5 O (top left), Ne (top middle), Mg (top right), Si (bottom left), S (bottom middle), and Fe (bottom right) abundance (in units of solar abundance) maps of G292.0+1.8. Regions A/B/C/D as shown in Figure 1 are marked here.

column density map is relatively uniform, suggesting no extra absorbing materials around this SNR. The temperatures are typically $0.5 - 1.0$ keV. The relatively “hot” regions are those around the pulsar wind nebula, and the “high” temperatures could be not real but the contamination of the non-thermal emission from the pulsar wind nebula. The central bright belt of G292.0+1.8 was attributed to the forward shocked circumstellar medium (Park et al. 2002), which should have larger electron density (n_e) and longer shocked time (t). Its ionization age ($\text{Log}_{10} n_e t$), however, is even smaller than other region. The reason might be that these materials have reached ionization equilibrium, and the ionization age we give here is obtained from non-equilibrium model and thus not reliable for these regions.

The spatial distribution of all the fitted elements are shown in Figure 5. It is clear that the central barlike structure is not enhanced in any of these element. This supports its origin of circumstellar materials (Park et al. 2004; Ghavamian, Hughes & Williams 2005). In the meantime, no clear stratification of the element abundances are observed from these maps. The distribution of the Ne and Si enhanced regions are generally consistent with their EW maps obtained by Park et al. (2002).

(II) The correlations of the element abundance.

Figure 6 shows the correlation plots of the abundances of O & Ne with the other elements, and Figure 7 shows the correlation of Si & Fe with the others. The points with minimum element abundances ($\sim 20\%$ of the total data points, i.e., the very black regions in each of the panel of Figure 5) are excluded, for they represent regions with very weak metal emission lines and thus probably dominated by the continuum. The coherent coefficients (ρ) are given in Table 1, along with the corresponding values obtained in Cas A (Yang et al. 2008).

The first observation to Table 1 and Figure 6 – 7 is that in G292.0+1.8 the abundances of O, Ne & Mg are in good correlation with each other, and so is Si vs. S. Such a correlation pattern can also be found in Cas A (cf. Table 1), although the coherent coefficients are different. For example, the most correlated pair in G292.0+1.8 is Ne and Mg, with $\rho = 0.88$, while in Cas A this coefficient is 0.49. The second observation is that the Fe abundance is basically not correlated with that of any other element. However, the two phase correlation between Si and Fe abundance found in Cas A (Figure 8 in Yang et al. 2008) was not shown in G292.0+1.8. These will be discussed in Section 4.1.

4 DISCUSSION

4.1 Nucleosynthesis

The O, Ne, and Mg abundance show tight correlations with each other within the range of about two orders of magnitude. This is a strong evidence that they all come from the explosive C/Ne burning. Meanwhile, such correlation is also found between Si and S abundance, suggesting them to be ashes of explosive O-burning and incomplete Si-burning in the core-collapse supernova. This kind of correlation pattern for elemental abundance is very similar to Cas A (Yang et al. 2008), and also is consistent with the (explosive) nucleosynthesis calculations for massive star (Woosley, Heger & Weaver 2002; Woosley & Janka 2005). The difference between G292.0+1.8 and Cas A is that the former SNR is Oxygen-rich while the latter one is Si-rich.

In Cas A, the Fe abundance is positively correlated with that of Si when Si abundance is lower than 3 solar abundances, and a negative correlation appears when the Si abundance is higher (Yang et al. 2008). It is suggested that the Si-rich regions are the ejecta of incomplete explosive Si-burning mixing with O-burning products, and the regions with lower Si abundance might be dominated by the shocked circumstellar medium (CSM). In G292.0+1.8, we can only find a weak positive correlation between Si and Fe abundance in the whole remnant. This is not surprising because no prominent Fe lines have been detected in most of the “pixels” we divided for G292.0+1.8, and thus the Fe abundance can not be that well-constrained. In the meantime, both Si and Fe are not enriched in the SNR, with their abundances smaller than 1 solar abundance. This, again, confirms that the reverse shock may have not propagated into the Fe-rich ejecta (Park et al. 2004; Ghavamian et al. 2009; 2012).

4.2 Progenitor Mass

Theoretical calculations suggested that for core-collapse supernovae the different progenitor mass will yield very different abundance pattern (Woosley & Weaver 1995, etc). Gonzalez & Safi-Harb (2003) suggested that the progenitor mass of G292.0+1.8 could be around $30 - 40 M_{\odot}$ based on the comparison of the observed abundance ratios with theoretical values. Their abundance ratios are taken from several ejecta-dominated regions within this SNR.

Here we gave the emission measure weighted average abundance for O, Ne, Mg, Si, S, and Fe among the whole remnant and their rms (Z and σ_Z in Table 2). To compare with GS03 work, we also give the abundance ratio of all the elements with respect to Si and their rms (Z/Z_{Si} and $\sigma_{Z/Z_{Si}}$ in Table 2). By taken G03’s observational value and theoretical values they employed, we overplotted our measurements in Figure 8. The abundance ratios measured here are systematically lower than those from GS03. One would wonder that the reason could be that the shocked CSM regions are included in our calculation. Considering this, we artificially choose the ejecta-dominated region by the standard of the O abundance larger than 1.0, and calculated the corresponding ratio again (Table 2, $(Z/Z_{Si})'$). We can

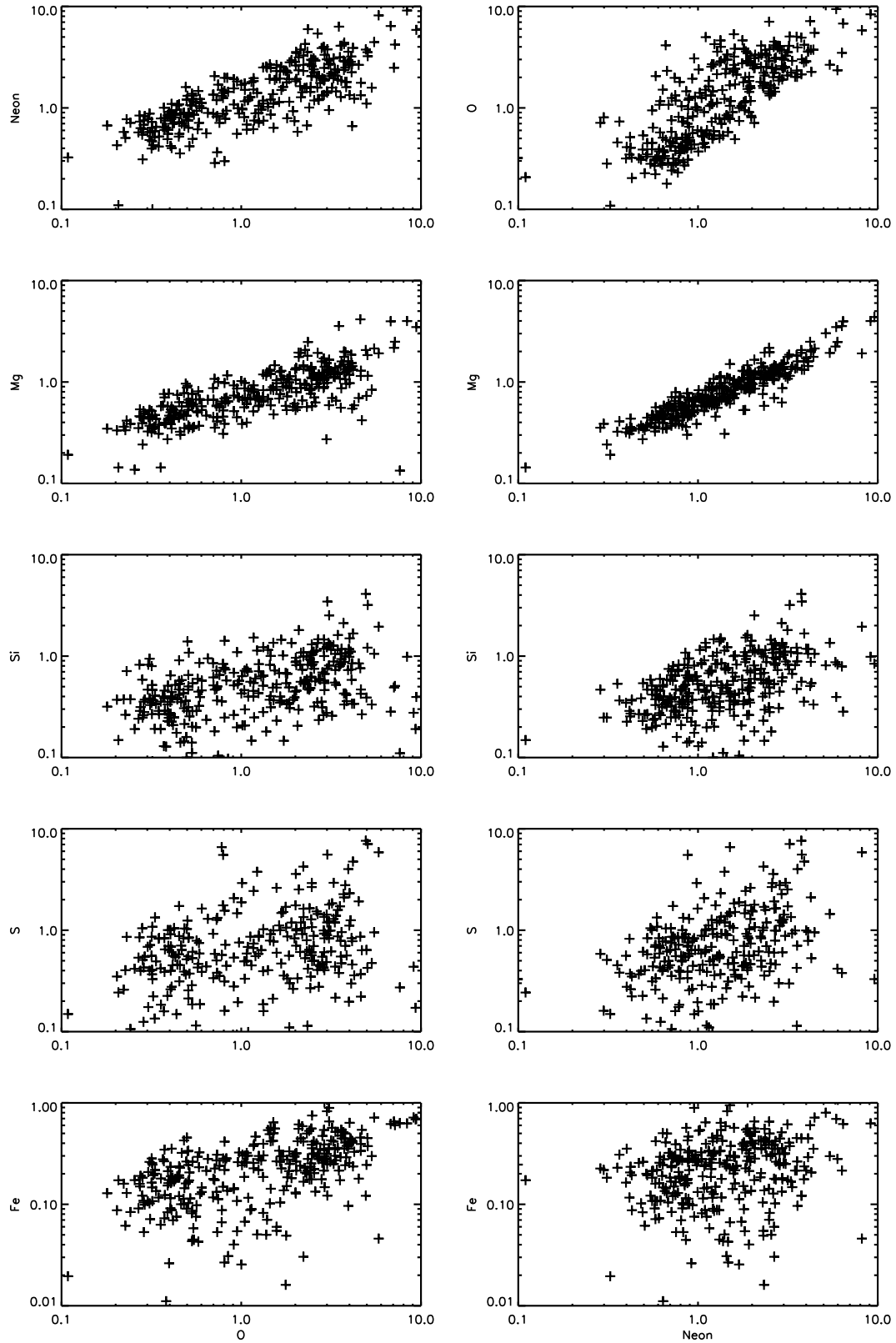


Fig. 6 Abundance correlation between O/Ne and the other elements.

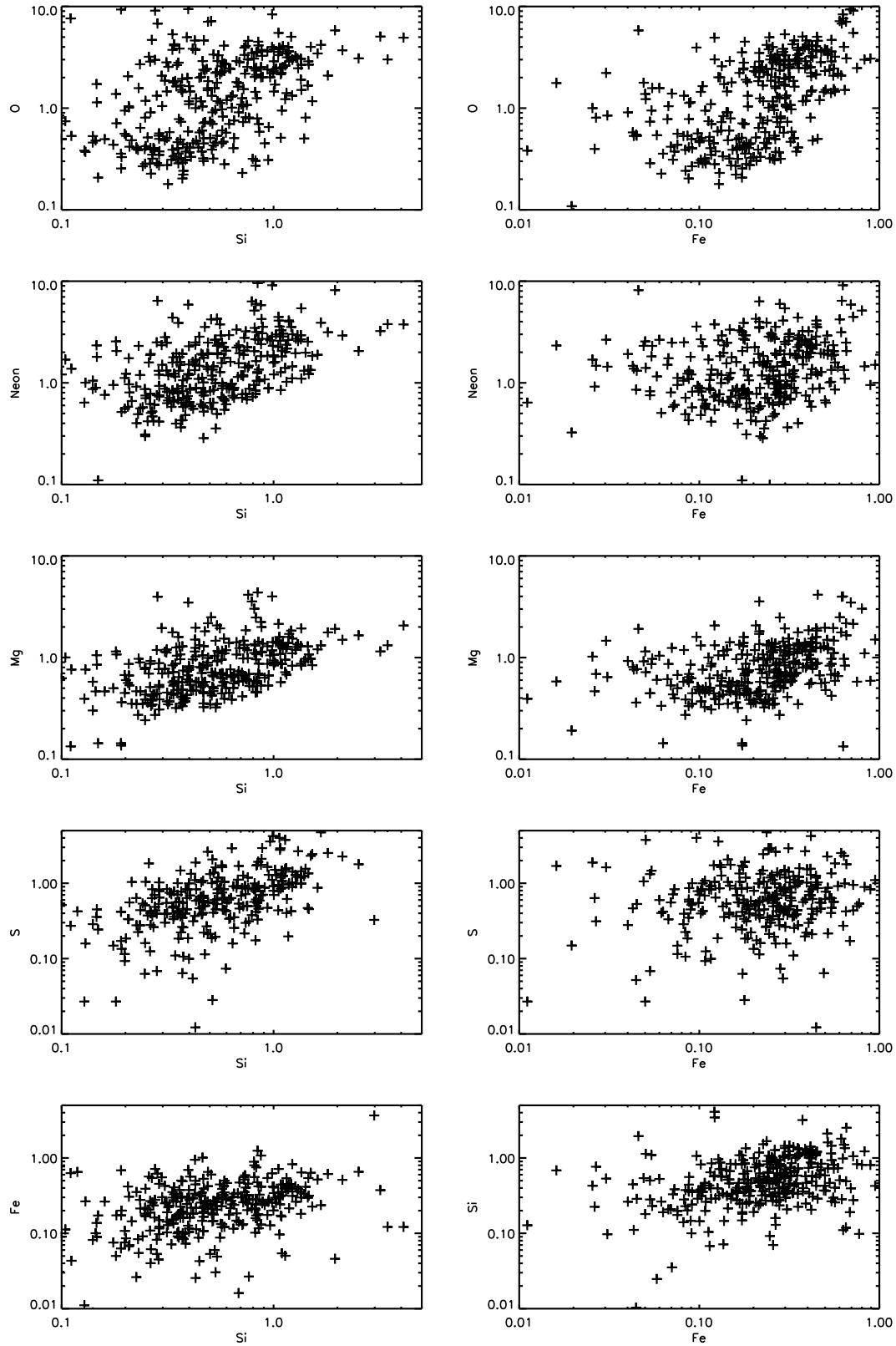


Fig. 7 Abundance correlation between Si/Fe and the other elements.

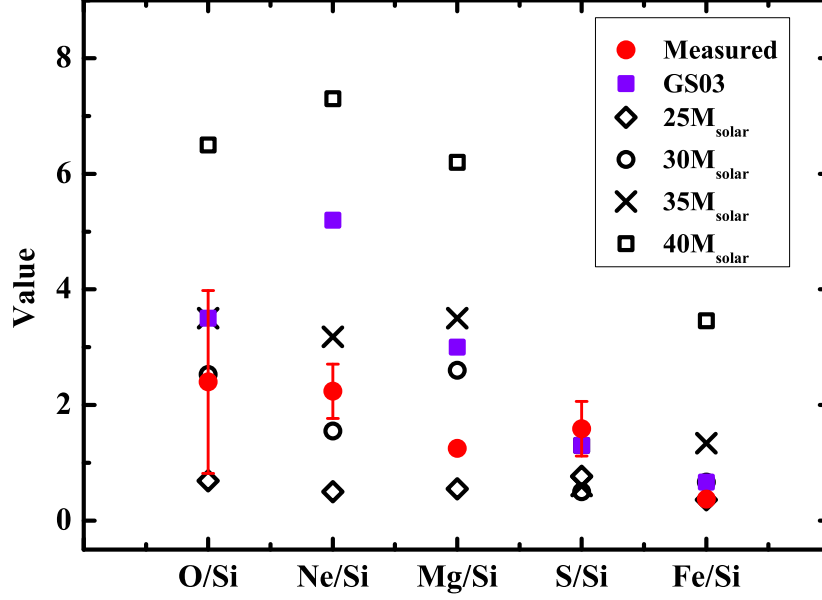


Fig. 8 Average abundance ratio and their rms scatter, compared with Gonzalez & Safi-Harb (2003) and theoretical values.

see that $(Z/Z_{Si})'$ are generally consistent with Z/Z_{Si} within the scatter. This is not surprising for two reasons. One is that the Si abundance are tentatively correlated with other elements. The other is that the larger element abundance values contribute much more to the final average values, so that even though the average abundance are much larger, their ratios tend to be similar. Our measurements suggested the progenitor mass for G292.0+1.8 to be 25 – 30 M_{\odot} , smaller than 30 – 40 M_{\odot} suggested by GS03.

5 SUMMARY

We did a spatially resolved X-ray spectroscopy of the SNR G292.0+1.8. The spatial distribution of the absorption column density, temperature, ionization age, and the abundances of O, Ne, Mg, Si, S and Fe are given. The uniform column density map suggests no extra absorbing material around this SNR. The central bright belt (with larger electron density and longer shocked time) show smaller ionization age than other regions. All of the element abundance maps show no clear stratification. The central barlike structure is not enhanced in any of the element abundance, supporting its origin of shocked circumstellar material. The Fe emission lines are not prominent among the whole remnant, and its abundance are significantly deduced, indicating that the reverse shock may have not propagated to the Fe-rich ejecta. The O/Ne/Mg abundances show tight correlation with each other, and so do Si/S. Such correlation suggests a common origin of nucleosynthesis for O/Ne/Mg and Si/S respectively. Based on relative abundances of O, Ne, Mg, Si and Fe to Si, we suggest a progenitor mass of 25 – 30 M_{\odot} for G292.0+1.8.

Acknowledgements We acknowledge the use of data obtained by Chandra. The Chandra Observatory Center is operated by the Smithsonian Astrophysical Observatory for and on the behalf of NASA. This project is supported by the National Natural Science Foundation of China under Nos. 10903007 and 11273022.

References

- Arnaud, K. A. 1996, ASPC, 101, 17
- Anders, E., & Grevesse, N. 1989, *Geochimica et Cosmochimica Acta*, 53, 197
- Becker, W. 2009, ASSL, 357, 91
- Borkowski, K. J., Lyerly, W. J., & Reynolds, S. P. 2001, *ApJ*, 548, 820
- Camilo, F., Manchester, R. N., Gaensler, B. M., Lorimer, D. R., & Sarkissian, J. 2002, *ApJ*, 567, L71
- Gaensler, B. M., & Wallace, B. J. 2003, *ApJ*, 594, 326
- Ghavamian, P., Hughes, J. P., & Williams, T. B. 2005, 635, 365
- Ghavamian, P., Long, K. S., Blair, W. P., Park, S., Fesen, R., Gaensler, B. M., Hughes, J. P., Rho, J., & Winkler, P. F., 2012, *ApJ*, 750, 39
- Ghavamian, P., Raymond, J. C., Blair, W. P., Long, K. S., Tappe, A., Park, S., & Winkler, P. F. 2009, *ApJ*, 696, 1307
- Goss, W. M., Shaver, P. A., Zealey, W. J., Murdin, P., & Clark, D. H. 1979, *MNRAS*, 188, 357
- Gonzalez, M., & Safi-Harb, S. 2003, *ApJ*, 583, L91
- Hughes, J. P., & Singh, K. P. 1994, *ApJ*, 422, 126
- Hughes, J. P., Slane, P. O., Burrows, D. N., Garmire, G., Nousek, J. A., Olbert, C. M., & Keohane, J. W. 2001, *ApJ*, 559, L153
- Hughes, J. P., Slane, P. O., Park, S., Roming, P. W. A., & Burrows, D. N. 2003, *ApJ*, 591, L139
- Lee, J. J., Park, S., Hughes, J. P., Slane, P. O., Gaensler, B. M., Ghavamian, P., & Burrows, D. N., 2010, *ApJ*, 711, L861
- Morrison, R., & McCammon, D. 1983, *ApJ*, 270, 119
- Murdin, P., & Clark, D. H. 1979, *MNRAS*, 189, 501
- Park, S., Roming, P. W. A., Hughes, J. P., Slane, P. O., Burrows, D. N., Garmire, G. P., & Nousek, J. A. 2002, *ApJ*, 564, L39
- Park, S., Hughes, J. P., Slane, P. O., Burrows, D. N., Roming, P. W. A., Nousek, J. A., & Garmire, G. P. 2004, *ApJ*, 602, L33
- Park, S., Hughes, J. P., Slane, P. O., Burrows, D. N., Gaensler, B. M., & Ghavamian, P. 2007, *ApJ*, 670, L121
- Tuohy, I. R., Burton, W. M., & Clark, D. H. 1982, *ApJ*, 260, L65
- Vink, J., Bleeker, J., Kaastra, J. S., & Rasmussen, A. 2004, *NuPhS*, 132, 62
- Woosley, S. E., Heger, A., & Weaver, T. A. 2002, *Rev. Mod. Phys.*, 74, 1015
- Woosley, S. E., & Janka, T. 2005, *Nat. Phys.*, 1, 147
- Woosley, S. E., & Weaver, T. A. 1995, *ApJS*, 101, 181
- Yang, X. J., Lu, F. J., & Chen, L. 2008, *ChJAA*, 4, 439

Table 1 coherent coefficient for data points excluding extremum ones. The corresponding value for Cas A (Yang et al. 2008) are given in parentheses.

Element	O	Ne	Mg	Si	S	Fe
O	—	0.64(0.33)	0.66(0.41)	0.58(0.33)	0.45(0.26)	0.43(0.13)
Ne	0.64(0.33)	—	0.88(0.49)	0.47(0.19)	0.41(0.16)	0.03(0.25)
Mg	0.66(0.41)	0.88(0.49)	—	0.52(0.48)	0.29(0.39)	0.24(0.24)
Si	0.58(0.33)	0.47(0.19)	0.52(0.48)	—	0.70(0.86)	0.31(0.23)
S	0.45(0.26)	0.41(0.16)	0.29(0.39)	0.70(0.86)	—	0.01(0.11)
Fe	0.43(0.13)	0.03(0.25)	0.24(0.24)	0.31(0.23)	0.01(0.11)	—

Table 2 Emission measure weighted average abundance and their ratios with respect to Si.

Element	O	Ne	Mg	Si	S	Fe
Z	1.32	1.24	0.69	0.55	0.88	0.20
σ_Z	1.03	0.41	0.09	0.07	0.38	0.01
Z/Z_{Si}	2.40	2.24	1.25	—	1.59	0.37
$\sigma_{Z/Z_{Si}}$	1.58	0.47	0.01	—	0.47	0.03
$(Z/Z_{Si})'$	3.29	2.54	1.30	—	1.53	0.35

Z : emission measure weighted average abundance;

σ_Z : weighted standard deviation for Z ;

Z/Z_{Si} : elemental abundance ratio with respect to Si;

$\sigma_{Z/Z_{Si}}$: standard deviation for Z/Z_{Si} ;

$(Z/Z_{Si})'$: emission measure weighted average abundance for the regions with O abundance greater than 1.0.